Highly indistinguishable heralded single-photon sources using parametric down conversion

Masato Tanida,[1,2] **Ryo Okamoto,**[1,2] **and Shigeki Takeuchi**[1,2,*]

[1]*The Institute of Scientific and Industrial Research, Osaka University, Ibaraki 567-0047, Japan*

[2]*Research Institute for Electronic Science, Hokkaido University, Sapporo 001-0021, Japan*

[*]*takeuchi@es.hokudai.ac.jp*

Abstract: We theoretically and experimentally investigate the conditions necessary to realize highly indistinguishable single-photon sources using parametric down conversion. The visibilities of Hong–Ou–Mandel (HOM) interference between photons in different fluorescence pairs were measured and a visibility of 95.8 $\pm$ 2% was observed using a 0.7-mm-long beta barium borate crystal and 2-nm bandpass filters, after compensating for the reflectivity of the beam splitter. A theoretical model of HOM interference visibilities is proposed that considers non-uniform down conversion process inside the nonlinear crystal. It well explains the experimental results.

OCIS codes: (270.5585) Quantum information and processing; (270.5290) Photon statistics.

References and links

1. C. H. Bennett and G. Brassard, "Quantum cryptography: public key distribution and coin tossing," Proceedings of IEEE International Conference on Computers Systems and Signal Processing 175–179 (1984).
2. M. A. Nielsen and I. L. Chuang, *Quantum Computation and Quantum Information*, (Cambridge University Press, Cambridge, England, 2000).
3. V. Giovannetti, S. Lloyd, and L. Maccone, "Quantum-enhanced measurements: beating the standard quantum limit," Science **306**, 1330–1336 (2004).
4. E. Knill, R. Laflamme, and G. J. Milburn, "A scheme for efficient quantum computation with linear optics," Nature (London) **409**, 46–52 (2001).
5. C. K. Hong, Z. Y. Ou, and L. Mandel, "Measurement of subpicosecond time intervals between two photons by interference," Phys. Rev. Lett. **59**, 2044–2046 (1987).
6. T. C. Ralph, N. K. Langford, T. B. Bell, and A. G. White, "Linear optical controlled-NOT gate in the coincidence basis," Phys. Rev. A **65**, 062324 (2002).
7. H. F. Hofmann and S. Takeuchi, "Quantum phase gate for photonic qubits using only beam splitters and postselection," Phys. Rev. A **66**, 024308 (2002).
8. J. L. O'Brien, G. J. Pryde, A. G. White, T. C. Ralph, and D. Branning, "Demonstration of an all-optical quantum controlled-NOT gate," Nature (London) **426**, 264–267 (2003).
9. N. K. Langford, T. J. Weinhold, R. Prevedel, K. J. Resch, A. Gilchrist, J. L. O'Brien, G. J. Pryde, and A. G. White, "Demonstration of a simple entangling optical gate and its use in Bell-state analysis," Phys. Rev. Lett. **95**, 210504 (2005).
10. N. Kiesel, C. Schmid, U. Weber, R. Ursin, and H. Weinfurter, "Linear optics controlled-phase gate made simple," Phys. Rev. Lett. **95**, 210505 (2005).
11. R. Okamoto, H. F. Hofmann, S. Takeuchi, and K. Sasaki, "Demonstration of an optical quantum controlled-NOT gate without path interference," Phys. Rev. Lett. **95**, 210506 (2005).
12. R. Okamoto, J. L. O'Brien, H. F. Hoffman, T. Nagata, K. Sasaki, and S. Takeuchi, "An entanglement filter," Science **323**, 483–485 (2009).
13. B. P. Lanyon, M. Barbieri, M. P. Almeida, T. Jennewein, T. C. Ralph, K. J. Resch, G. J. Pryde, J. L. O'Brien, A. Gilchrist, and A. G. White, "Simplifying quantum logic using higher-dimensional Hilbert spaces," Nat. Phys. **5**, 134–140 (2009).

#167018 - $15.00 USD Received 18 Apr 2012; revised 25 May 2012; accepted 29 May 2012; published 22 Jun 2012

14. R. Okamoto, J. L. O'Brien, H. F. Hofmann, and S. Takeuchi, "Realization of a Knill-Laflamme-Milburn C-NOT gate a photonic quantum circuit combining effective optical nonlinearities," Proc. Natl. Acad. Sci. USA **108**, 10067–10071 (2011).
15. H. Lee, P. Kok, and J. P. Dowling, "A quantum Rosetta stone for interferometry," J. Mod. Opt. **49**, 2325–2338 (2002).
16. T. Nagata, R. Okamoto, J. L. O'Brien, K. Sasaki, and S. Takeuchi, "Beating the standard quantum limit with four-entangled photons," Science **316**, 726–729 (2007).
17. N. Boto, P. Kok, D. S. Abrams, S. L. Braunstein, C. P. Williams, and J. P. Dowling, "Quantum interferometric optical lithography: exploiting entanglement to beat the diffraction limit," Phys. Rev. Lett. **85**, 2733–2736 (2000).
18. Y. Kawabe, H. Fujiwara, R. Okamoto, K. Sasaki, and S. Takeuchi, "Quantum interference fringes beating the diffraction limit," Opt. Express **15**, 14244–14250 (2007).
19. T. Nagata, R. Okamoto, H. F. Hofmann, and S. Takeuchi, "Analysis of experimental error sources in a linear-optics quantum gate," New J. Phys. **12**, 043053 (2010).
20. T. Jennewein, R. Ursin, M. Aspelmeyer, and A. Zeilinger, "Performing high-quality multi-photon experiments with parametric down-conversion," J. Phys. B **42**, 114008 (2009).
21. P. R. Tapster and J. G. Rarity, "Photon statistics of pulsed parametric light," J. Mod. Opt. **45**, 595–604 (1998).
22. H. R. Zhang and R. P. Wang, "Theory of fourfold interference with photon pairs from spatially separated sources," Phys. Rev. A **75**, 053804 (2007).
23. M. Barbieri, "Effects of frequency correlation in linear optical entangling gates operated with independent photons," Phys. Rev. A **76**, 043825 (2007).
24. R. Kaltenbaek, R. Prevedel, M. Aspelmeyer, and A. Zeilinger, "High-fidelity entanglement swapping with fully independent sources," Phys. Rev. A **79**, 040302(R) (2009).
25. M. Zukowski, A. Zeilinger, and H. Weinfurter, "Entangling independent pulsed photon sources," Ann. N.Y. Acad. Sci. **755**, 91–102 (1995).
26. R. Kaltenbaek, B. Blauensteiner, M. Zukowski, M. Aspelmeyer, and A. Zeilinger, "Experimental interference of independent photons," Phys. Rev. Lett. **96**, 240502 (2006).
27. R. Kaltenbaek, 2008 PhD Thesis.
28. S. M. Saltiel, K. Koynov, B. Agate, and W. Sibbett, "Second-harmonic generation with focused beams under conditions of large group-velocity mismatch," J. Opt. Soc. Am. B **21**, 591–598 (2004).
29. Y. Kawabe, H. Fujiwara, S. Takeuchi, and K. Sasaki, "Investigation of the spatial propagation properties of type-I parametric fluorescence by use of tuning curve filtering method," Jpn. J. Appl. Phys. **46**, 5802–5808 (2007).

1. Introduction

Quantum information technology exploits fundamental phenemena of quantum mechanics such as quantum entanglement and the uncertainty principle to realize novel functional applications, including quantum key distribution [1], quantum computation [2], and quantum metrology [3]. Photons are the most useful particles for these applications because they can be transmitted over long distances without decoherence via optical fibers or the atmosphere, they can be easily detected by conventional technologies, and they can be manipulated with high precision using developed optical devices. However, the lack of interaction between photons has hindered their use in such applications.

To overcome this problem, Knill, Laflamme, and Milburn (KLM) [4] found that it is possible to effectively generate the required interaction between single photons using Hong–Ou–Mandel (HOM) interference [5], which is a two-photon interference at a beam splitter. Based on this concept, controlled-NOT gates for photonic qubits were proposed [6, 7] and demonstrated [8–11]. Furthermore, small-scale optical quantum circuits [12,13], including the original proposal for heralded controlled-NOT operation by KLM [14], have been demonstrated. HOM interference is also important for generating NOON states [15] used in quantum metrology [16] and quantum lithography [17, 18].

For these applications, it is very important to develop highly indistinguishable single-photon sources that can generate high-visibility HOM interference. In the previous demonstrations, the HOM visibilities (86% [12] and 90% [14]) of the heralded single photon sources strongly limited the performance of the quantum circuits [19].

In this paper, we theoretically and experimentally investigate the conditions for realizing highly indistinguishable heralded single-photon sources using spontaneous parametric down

#167018 - $15.00 USD Received 18 Apr 2012; revised 25 May 2012; accepted 29 May 2012; published 22 Jun 2012

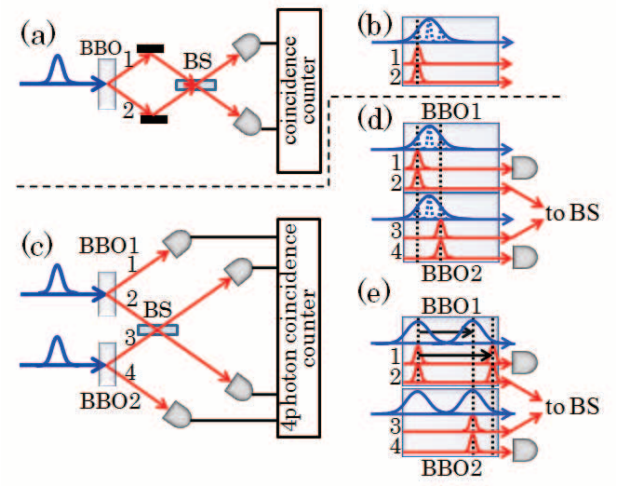

Fig. 1. (a) Schematic of Hong-Ou-Mandel interferometer between photons in a pair. (b) Since photons in a pair are generated from a single pump photon, no timing-jitter occurs. (c) Schematic of Hong-Ou-Mandel interferometer between photons in different pairs. (d) The timing-jitter caused by non-zero pulse duration. The photon pairs are generated in the front side (left side) in BBO1 and in the back side (right side) in BBO2. Thus, the input photons has the timing jitter. (e) The timing-jitter caused by GVM. Since the daughter photons propagate faster than the pump light (GVM), the timing-jitter occurs between photons in different pairs.

conversion (SPDC). We consider a case in which photons are generated at the same wavelength by type-I down conversion, which is commonly used in experiments [12, 13, 16]. In a previous analysis [20] of the same conditions, photon pairs were assumed to be uniformly generated in a crystal; i.e., the conversion efficiency was assumed to remain constant as the pump pulse propagates through the crystal. Here, we extend the theory by considering that the number of photon pairs increases linearly as the pump propagates within the crystal [21]. As we show later, this effect becomes significant for crystal lengths of about 1.5 mm or longer, which have been commonly used in previous experiments [12, 13, 15]. Other theoretical studies have investigated different conditions (e.g., non-degenerate type-I [22] and degenerate type-II [23] phase-matching conditions).

We also experimentally investigate the effect of group velocity mismatch (GVM) in crystals by using crystals with different lengths (0.7 and 1.5 mm); this has not been experimentally investigated previously. We succeeded in obtaining a high-visibility of $95.8 \pm 2\%$ after compensating for the reflectivity of the beam splitter (observed value: $95.2 \pm 2\%$) using a 0.7-mm-long beta barium borate (BBO) crystal and a 2-nm bandpass filters. To the best of our knowledge, this visibility equals the highest visibility ever reported [24], but in our case the coincidence rates were higher by a factor of 4. Numerical calculations based on our extended theory agree well with the experimental results.

The paper is organized as follows. In section 2, we introduce the theory for the visibility of HOM dips that considers the pulse width of the pump laser and the GVM between the pump laser and generated pairs. In section 3, we describe the experimental setup used. Section 4 presents the experimental results for HOM interference between photons in same and different pairs and compares them with the results of theoretical calculations.

#167018 - $15.00 USD Received 18 Apr 2012; revised 25 May 2012; accepted 29 May 2012; published 22 Jun 2012

2. Theoretical model

We assume that the shape of the HOM dips can be described by [5]

$$N(\delta\tau) = N_{max}\left(1 - V \times e^{-\left(\frac{\delta\tau}{\tau_c}\right)^2}\right), \tag{1}$$

where $N(\delta\tau)$ is the coincidence counts, $\delta\tau$ is the optical delay time between the photons, N_{max} is the maximum coincidence counts, V is the visibility of the HOM dip, and τ_c is the coherence time of the input photons. Here, we assume that the input two photons have the same wavelength and the same coherence time.

To clarify the nature of single-photon sources, we discuss two-photon interference visibilities $\tilde{V}$ for an ideal reflectivity of 50%. However, the reflectivity R of a beam splitter (BS) in actual experiments is not exactly 50%. The visibility $\tilde{V}$ for the ideal reflectivity can be calculated from the measured visibility V using

$$\tilde{V} = \frac{2R^2 - 2R + 1}{2R - 2R^2} \times V. \tag{2}$$

2.1. Visibility of HOM dip between photons in a pair

We first discuss the visibility $\tilde{V_s}$ of HOM dips between photons in a pair which can be calculated from an experimentally measured V_s using Eq. (2). Spatial, temporal, or polarization mode mismatch between a pair of input photons can degrade the quality of HOM dips. However, unlike the case of two photons belonging to different pairs (which is discussed below), it is not necessary to consider undesirable timing jitters between the incident photons because the two photons are generated from a single pump photon and thus no timing jitter occurs for the type-I phase matching condition (Fig. 1(b)). In this context, $\tilde{V_s}$ is a useful parameter for evaluating the effect of mode mismatch on HOM dips.

2.2. Visibility of HOM dip between photons in different pairs

We now discuss how the visibility $\tilde{V_d}$ of HOM dips between photons in different pairs, which can be extracted from experimentally obtained V_d using Eqs. (1) and (2), can be predicted theoretically. As mentioned above, in this case it is necessary to consider both the mode mismatch and undesirable timing jitters between the input photons to estimate $\tilde{V_d}$. There are two main causes for undesirable timing jitters: a non-zero pump pulse duration (Fig. 1(d)) and a GVM between the pump pulse and the daughter photons (Fig. 1(e)). In this paper, we introduce the 'visibilities' V_{pump} and V_{GVM} to consider these two effects. In the first approximation, $\tilde{V_d}$ can be written as [20]

$$\tilde{V_d} = \tilde{V_s} \times V_{pump} \times V_{GVM}, \tag{3}$$

Figure 1(d) depicts the effect of the non-zero pump pulse duration. The upper and lower crystals in Fig. 1(d) correspond to BBO1 and BBO2 in Fig. 1(c), respectively. As Fig. 1(d) shows, the photon pairs are generated on the front (left) side of BBO1 and on the back (right) side of BBO2. Thus, the input photons have a timing jitter V_{pump}, which is given by [25–27].

$$V_{pump} = \sqrt{\frac{\tau_p^2\tau_t^2 + \tau_t^2\tau_i^2 + \tau_i^2\tau_p^2}{(\tau_p^2 + \tau_t^2)(\tau_p^2 + \tau_i^2)}} = \sqrt{1 - \frac{1}{\left(1 + \frac{\tau_t^2}{\tau_p^2}\right)\left(1 + \frac{\tau_i^2}{\tau_p^2}\right)}}. \tag{4}$$

Here, τ_p is the pump pulse duration, τ_t is the coherence time of the trigger photons (photons 1 and 4 in Fig. 1(c)), and τ_i is the coherence time of the input photons (photons 2 and 3 in Fig.

#167018 - $15.00 USD Received 18 Apr 2012; revised 25 May 2012; accepted 29 May 2012; published 22 Jun 2012

1(c)). Equation (4) suggests that V_{pump} can be maximized by increasing τ_i and τ_t with respect to τ_p. This is because the increase in τ_i and τ_t corresponds to the broadening of the width of the photonic wave packets of the signal and the idler photons (Fig. 1(d)) so that the effect of the timing jitter due to non-zero pump pulse duration is reduced. In experiments, the smaller the band width of the band pass filters for trigger and input photons are, the larger τ_i and τ_t are.

$\tilde{V_s}$ describes the effect of mode mismatch between the input photons, which can be estimated from the experimentally obtained V_s. V_{GVM} will be discussed in detail in the following section.

2.3. Visibility degradation due to group velocity mismatch

Figure 1(e) shows a schematic for the effect of GVM. Again, the upper and lower crystals in Fig. 1(e) correspond to BBO1 and BBO2 in Fig. 1(c), respectively. As Fig. 1(e) shows, photon pairs are generated when the pump pulse enters BBO1 (left side), whereas they are generated when the pump pulse exits BBO2 (right side). Since the daughter photons propagate faster than the pump light (GVM), the photon from BBO1 arrives at the BS sooner than the photon from BBO2 in this example.

The group delay between the pump pulse and the daughter photons is given by

$$\Delta u = \frac{1}{v_{ge}(\lambda/2)} - \frac{1}{v_{go}(\lambda)}, \tag{5}$$

where $v_{ge}(\lambda)$ and $v_{go}(\lambda)$ are respectively the group velocities of the extraordinary and ordinary rays for λ, which is the wavelength of the daughter photons.

To evaluate V_{GVM}, we calculate the HOM dip function $F(T,t)$ by accounting for the effect of timing jitters between the input photons as follows.

$$F(T,\delta\tau) = \int_0^T \int_0^T g(\tau)\, g(\tau') \left(1 - e^{-\left(\frac{\delta\tau-\tau-\tau'-T}{\tau_c}\right)^2}\right) \mathrm{d}\tau \mathrm{d}\tau', \tag{6}$$

where T is the maximum timing jitter ($T = L \times \Delta u$, where L is the crystal length), $g(\tau)$ is the photon pair creation rate at time τ after the pulse enters the crystal, and $\delta\tau$ is the optical delay time.

In a previous study [20], photon pairs were assumed to be uniformly generated in the crystal; in other words, the conversion efficiency was assumed to remain constant as the pump pulse propagates in a crystal. In this case, the photon pair creation rate $g(\tau)$ is given by:

$$g(\tau) = \left\{ \begin{array}{ll} 1 & (0 \le \tau \le L) \\ 0 & (\text{otherwise}) \end{array} \right\}. \tag{7}$$

If we follow this assumption, the number of photon pairs output from the crystal is proportional to the length of the crystal. However, when the SPDC process builds up coherently, the number of photon pairs output from the crystal should be quadratic to the length of the crystal [21]. In this case, the number of photon pairs generated at a point inside the crystal has to be proportional to the distance from the input end of the crystal. We think the latter case is more suitable for our experimental conditions where the Rayleigh length is much larger than the crystal length and the spatial walk off effect of the pump beam is not significant. Thus, in our extended theory, we replace $g(\tau)$ with

$$g(\tau) = \left\{ \begin{array}{ll} \tau & (0 \le \tau \le L) \\ 0 & (\text{otherwise}) \end{array} \right\}. \tag{8}$$

#167018 - $15.00 USD Received 18 Apr 2012; revised 25 May 2012; accepted 29 May 2012; published 22 Jun 2012

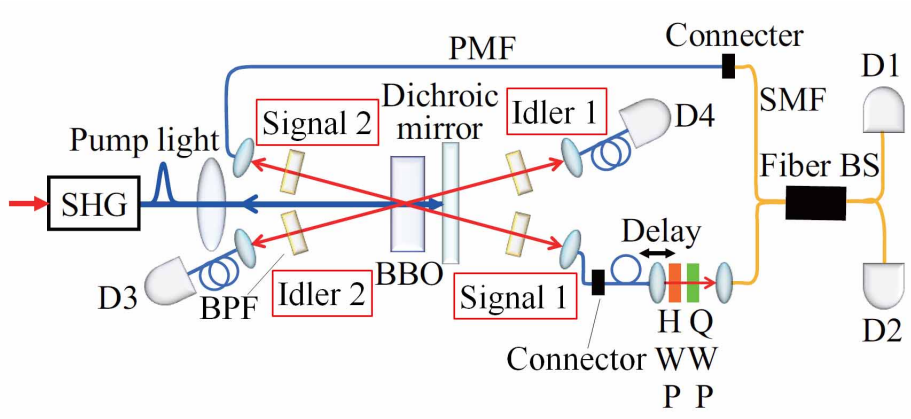

Fig. 2. Experimental setup of HOM interferometer between independent photons. SHG: second harmonic generation; PMF: polarization maintaining fiber; SMF: single-mode fiber; HWP (QWP): half (quarter) wave plate; SPCM: single-photon counting module.

Since V_{GVM} is the visibility of $F[T,\delta\tau]$,

$$V_{GVM} = 1 - \frac{\min[F(T,t),t]}{F[T,\infty]}. \tag{9}$$

Unfortunately, in our extended theory, $F[T,\delta\tau]$ is no longer a simple Gaussian function. Therefore, in this study, we numerically calculated the HOM dip function $F[T,\delta\tau]$ and searched for $\delta\tau$ which gives the minimum value to determine V_{GVM}.

3. Experimental setup

Figure 2 shows the experimental setup. A frequency-doubled mode-locked Ti:sapphire laser with an output wavelength of 390 nm and a repetition rate of 82 MHz is used as the pump light source. The frequency-doubled pump laser pulses are estimated to have a duration of 200 fs since the fundamental light was measured to have a pulse duration of 100 fs [28]. We used a BBO crystal for parametric down conversion for type-I phase-matching condition. In this experiment, we used BBO crystals with two different thicknesses (0.7 and 1.5 mm). The pump laser is loosely focused by a lens (f = 600 mm) so that the Rayleigh length is about 100 mm and the beam waist size at the focused spot is about 300 μm. As shown in Fig. 2, the pump beam is reflected by a dichroic mirror that is located 5 mm behind the crystal so that two pairs of parametric fluorescence photons are simultaneously generated in opposite directions. The angle between the pump and generated photons inside the crystal is set to 3.2 degrees. For this phase matching condition, the GVM between the pump (extraordinary ray) and daughter (ordinary ray) photons is 185 fs/mm. Note that for these thin crystals, the walk-off effect (about 50 and 100 μm for thicknesses of 0.7 and 1.5 mm, respectively) is much smaller than the pump beam waist size (300 μm) and can thus be neglected.

The four daughter photons (Signal 1 and 2 and Idler 1 and 2) are coupled to four polarization maintaining fibers (PMF: PMJ-3S3S-780-5/125-3, Oz Optics) via an objective lens and bandpass filters (FWHM 2-nm: specially ordered, Optoquest Co. Ltd., T_{max}=99%, CW=780 nm) (FWHM 4-nm: specially ordered, Barr Associates Inc, T_{max}= 92%, CW=780 nm). Note that we carefully selected filters that have the same center wavelength. We inserted an optical delay for Signal 1 to obtain a HOM dip. The half-wave plate (HWP) and the quarter-wave plate

#167018 - $15.00 USD Received 18 Apr 2012; revised 25 May 2012; accepted 29 May 2012; published 22 Jun 2012

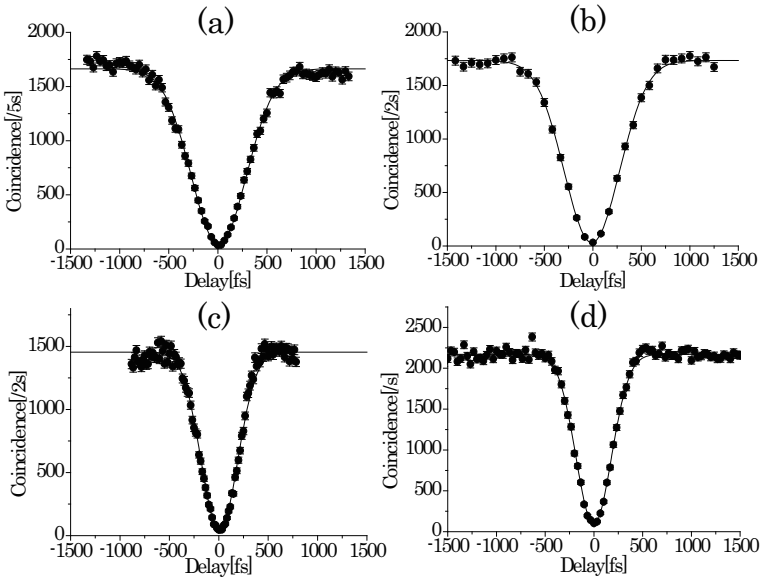

Fig. 3. HOM dips between daughter photons. The HOM dips are between Signal 1 and Idler 1 in Fig. 2 and with four different conditions (a) 0.7-mm BBO with 2-nm band-pass filters, (b) 0.7-mm BBO with 4-nm band-pass filters, (c) 1.5-mm BBO with 2-nm band-pass filters, and (d) 1.5-mm BBO with 4nm band-pass filters.

(QWP) inside the optical delay are adjusted to maximize the visibility of HOM dips. To obtain HOM dips for different pairs, we measured four-fold coincidence counts between four detectors D1 to D4 (SPCM-AQR13FC, Perkin Elmer) using a homemade coincidence circuit by varying the optical delay. To obtain HOM dips for a pair of photons, we measured two-fold coincidence counts between detectors D1 and D2 using similar experimental setups. For example, to obtain a HOM dip between Signal 2 and Idler 2, we coupled the PMF in the Idler 2 output to the connector immediately before the optical delay.

The beam splitting ratio R of the fiber beam splitter differs slightly from 50%; it depends on the bandwidth of the incident light. R was measured to be 47.2 and 46.2% for bandwidths of 2 and 4 nm, respectively. Each photon pair is guided into polarization maintaining fibers after being transmitted through BPFs of same bandwidth. The HOM dip is measured by varying the optical delay.

The FWHM of the spectrum of generated photon pairs coupled to a single mode fiber without inserting band pass filter was 70-nm for 1.5-mm long crystal. As is discussed in our former paper [29], the FWHM is determined mainly by the shape of the tuning curve and the acceptance angle of the objective lens of the fiber coupler. The thickness of the crystal determines the 'thickness' of the tuning curve. Thus, the FWHM could be slightly larger for 0.7-mm long crystal, may be $75 \sim 90$ nm.

4. Experimental results

4.1. HOM interference between a pair of daughter photons

We first measured HOM dips between a pair of daughter photons (Fig. 3). The HOM dips are between Signal 1 and Idler 1 (see Fig. 2) for the following four conditions: 0.7-mm BBO with

#167018 - $15.00 USD Received 18 Apr 2012; revised 25 May 2012; accepted 29 May 2012; published 22 Jun 2012

Table 1. Visibilities between photons in a pair for four conditions. S1: Signal 1; S2: Signal 2; I1: Idler 1; I2: Idler 2.

	condition(BBO, BPF)	V_s (S1,I1)	$\tilde{V}_s$	V_s (S2, I2)	$\tilde{V}_s$
(a)	0.7mm, 2nm	97.4 ± 0.2	98.0 ± 0.2	97.2 ± 0.2	97.8 ± 0.2
(b)	1.5mm, 2nm	98.3 ± 0.2	98.9 ± 0.2	97.2 ± 0.2	97.9 ± 0.2
(c)	0.7mm, 4nm	97.5 ± 0.3	98.6 ± 0.3	96.8 ± 0.4	97.9 ± 0.4
(d)	1.5mm, 4nm	96.7 ± 0.2	97.8 ± 0.2	96.7 ± 0.4	97.8 ± 0.4

	coherence time (S1, I1)	coherence time (S2, I2)
(a)	400 ± 4 fs	400 ± 3 fs
(b)	404 ± 4 fs	405 ± 5 fs
(c)	261 ± 3 fs	257 ± 3 fs
(d)	256 ± 2 fs	247 ± 3 fs

2-nm bandpass filters (Fig. 3(a)), 0.7-mm BBO with 4-nm bandpass filters (Fig. 3(b)), 1.5-mm BBO with 2-nm bandpass filters (Fig. 3(c)), and 1.5-mm BBO with 4-nm bandpass filters (Fig. 3(d)). The measured coincidence counts N are plotted as dots and the error bars are $\pm\sqrt{N}$. Note that even though we used relatively weak pump intensity (100 mW), we measured the contribution of multi-pair emission to the coincidence counts experimentally by closing one of the input port and subtracted them from the data shown in Fig. 3. The solid lines in the figures are fitting curves obtained using Eq. (1) with τ and V_s as free parameters.

Table 1 summarizes the fitting results. First, all the fitting results for both V_s and τ for the four conditions are the same for two different pairs (Signal 1, Idler 1 and Signal 2, Idler 2) within the errors. This implies that these two photon pair sources are almost identical. For V_s, we obtained average visibility $97.5 \pm 0.2\%$ with 2-nm bandpass filters and $96.9 \pm 0.4\%$ with 4-nm bandpass filters. After compensating for the non-ideal beam splitting ratio mentioned in the previous section using Eq. (3), $\tilde{V}_s = 98.2 \pm 0.2\%$ on average for a 2-nm bandpass filter, and $\tilde{V}_s = 98.0 \pm 0.3\%$ on average for 4-nm bandpass filters. These values are very close to unity; the slight deviations from unity may be caused by imperfect frequency or polarization mode matching.

4.2. HOM interference between photons in different pairs

Using a pump laser power of 200 mW, we measured HOM dips between photons in different pairs (Fig. 4) for the following four conditions: 0.7-mm BBO with 2-nm bandpass filters (Fig. 4(a)), 0.7-mm BBO with 4-nm bandpass filters (Fig. 4(b)), 1.5-mm BBO with 2-nm bandpass filters (Fig. 4(c)), and 1.5-mm BBO with 4-nm bandpass filters (Fig. 4(d)). Note that we subtracted the components due to the multi-pair emission from the coincidence counts as we mentioned in Sec. 4.1. The dots indicate the measured four-fold coincidence counts and the error bars are the square roots of the counts. The solid lines in Fig. 4 are fitting curves obtained using Eq. (1) with τ and V_d as free parameters.

The fitting results are summarized in Table 2. For $\tilde{V}_d$, we obtained $95.8 \pm 2\%$ for the case with a 0.7-mm-long crystal and a 2-nm bandpass filter. To the best of our knowledge, this visibility equals the highest visibility ever reported [24], but in the present case the coincidence rates were higher by a factor of 4.

Using a longer crystal (1.5 mm) and the same bandpass filter (2 nm), $\tilde{V}_d$ decreased to $91.9 \pm 2\%$ due to the larger GVM mismatch. With wider bandpass filters, $\tilde{V}_d$ for 0.7 and 1.5-mm-long crystals are $90.9 \pm 2\%$ and $83.7 \pm 2\%$, respectively.

#167018 - $15.00 USD Received 18 Apr 2012; revised 25 May 2012; accepted 29 May 2012; published 22 Jun 2012

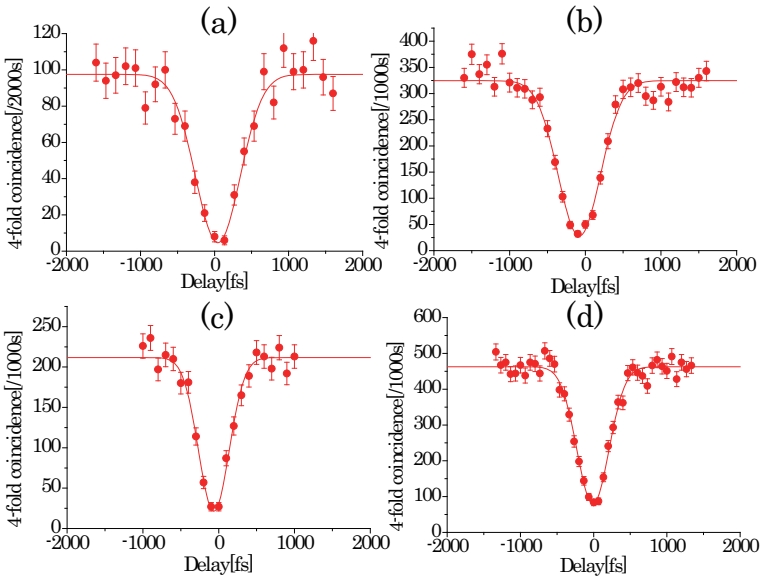

Fig. 4. HOM dips between photons in different pairs. (a) 0.7-mm BBO with 2-nm band-pass filters, (b) 0.7-mm BBO with 4-nm band-pass filters, (c) 1.5-mm BBO with 2-nm band-pass filters, and (d) 1.5-mm BBO with 4nm band-pass filters.

Table 2. Visibilities between different photon pairs for four conditions. S1: Signal 1; S2: Signal 2; I1: Idler 1; I2: Idler 2.

	condition(BBO, BPF)	V_d (S1, I2)	$\tilde{V}_d$	coherence time (S1, I1)
(a)	0.7mm, 2nm	95.2 ± 2.0	95.8 ± 2.0	428 ± 26 fs
(b)	1.5mm, 2nm	91.3 ± 1.5	91.9 ± 1.2	396 ± 16 fs
(c)	0.7mm, 4nm	89.8 ± 1.6	90.9 ± 1.8	286 ± 13 fs
(d)	1.5mm, 4nm	82.7 ± 1.2	83.7 ± 1.2	309 ± 10 fs

4.3. Comparison of theoretical model and experimental results

Figure 5 shows a plot of the visibilities $\tilde{V}_d$ of HOM dips between photons in different pairs. The horizontal and vertical axes represent the BBO crystal length and $\tilde{V}_d$, respectively. The blue and red dots represent data obtained using the 2 and 4-nm bandpass filters, respectively. The blue and red solid lines are plots of Eq. (3) for the cases with 2 and 4-nm bandpass filters, respectively. Since the GVM for the phase matching condition used is 185 fs/mm, T in Eq. (9) is 130 and 278 fs for 0.7 and 1.5-mm long crystals, respectively. We used the average $\tilde{V}_s$ of 98.2 % and 98.0 % (Sec. 4.1) for 2 and 4-nm bandpass filters, respectively. To calculate V_{pump} in Eq. (5), we used the estimated coherence times of the signal and idler photons in Table 1 (402 fs and 255 fs for 2 and 4-nm bandpass filters, respectively) for both τ_t and τ_i, and we set τ_p = 200 fs.

The theoretical curve fits the experimental data well for cases with both 2-nm (blue) and 4-nm (red) bandpass filters. The intersection points of the theoretical curves with the vertical axis is determined by $\tilde{V}_s$, which reflects the effect of mode mismatch between the input photons,

#167018 - $15.00 USD Received 18 Apr 2012; revised 25 May 2012; accepted 29 May 2012; published 22 Jun 2012

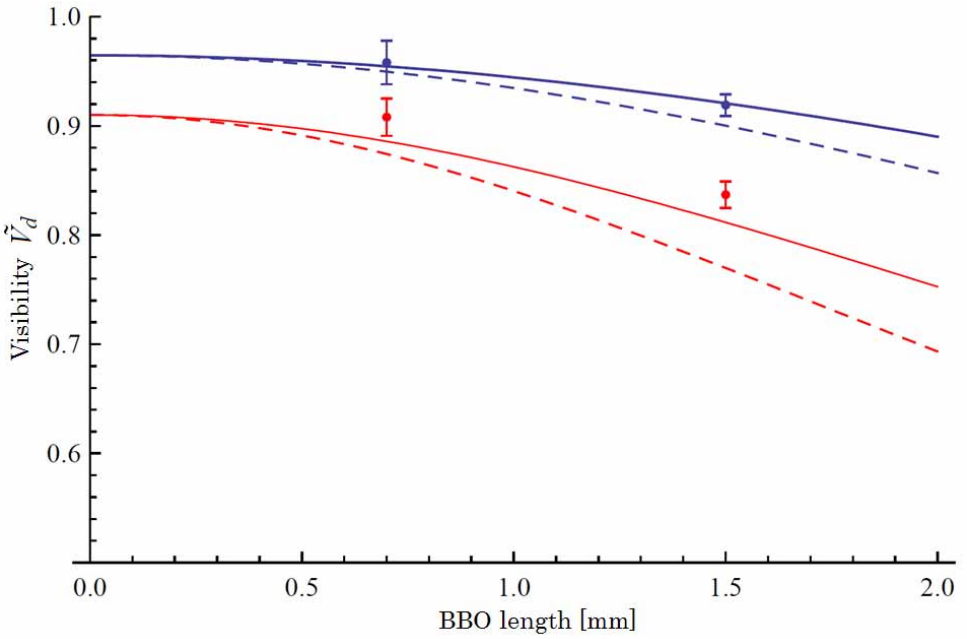

Fig. 5. Relationship between GVM and coherence time of interfering photons. Blue and red lines are $\tilde{V}_d$ at BPF = 2 and 4 nm, respectively. The dotted lines show the cases where SPDC occurs uniformly throughout the crystal [20].

and V_{pump}, which is determined by the effect of the timing jitter due to non-zero pump pulse duration (Fig. 1(d)). The difference of the intersection points between the two theoretical curves is due to V_{pump}. As we discussed in Sec. 2.2, V_{pump} is larger when the band widths of the band pass filters for trigger and input photons are smaller. Because of the broadening of the width of the photonic wave packets of the signal and the idler photons, the different wave packets can still overlap in spite of the timing jitter (Fig. 1(d)).

The decrease in $\tilde{V}_d$ as the crystal length increase is determined by V_{GVM}, the effect of GVM inside the crystal (Fig. 1(e)). When the crystal is longer, the timing jitter caused by GVM becomes significant, resulting in the reduction in the visibility. However, the deterioration is somewhat moderate for the blue solid line (BPF = 2nm) when compared to the red solid line (BPF = 4nm). This is because the photonic wave packets of the signal and the idler photons with the broadened width (BPF = 2nm) can overlap better.

The dotted lines show the cases where SPDC occurs uniformly throughout the crystal [20]. Naturally the discrepancy between the solid (the present theory, which assumes non-uniform generation) and dotted line increases with increasing crystal length; it becomes significant (5% for 4-nm bandpass filter) at a crystal length of 1.5 mm. For larger crystals length ($\geq$ 2 mm), the spatial walk off effect of the pump beam will be no more negligible and the SPDC process cannot build up coherently, and thus Eq. (8) is no more a good approximation. In this case, the experimentally observable $\tilde{V}_d$ will be between the solid and dotted lines.

5. Conclusion

We investigated the conditions for realizing highly indistinguishable single-photon sources using parametric down conversion both theoretically and experimentally. The visibilities of HOM

#167018 - $15.00 USD Received 18 Apr 2012; revised 25 May 2012; accepted 29 May 2012; published 22 Jun 2012

interference between photons in different fluorescence pairs were found to be 95.8 $\pm$ 2% after compensating for the reflectivity of the beam splitter (observed value: 95.2 $\pm$ 2%) using a 0.7-mm-long BBO crystal and a 2-nm bandpass filter. A theoretical model for HOM interference visibilities was proposed that considers non-uniform down conversion process inside the nonlinear crystal. It agreed well with the experimental results.

Acknowledgments

The authors would like to thank Professor N. Imoto and Professor M. Koashi for discussions. This work is supported in part by MEXT-KAKENHI Quantum Cybernetics (No. 21101007), JSPS-KAKENHI (Nos. 20244062, 23244079), JST-CREST, JSPS-FIRST, MIC-SCOPE, Project for Developing Innovation Systems of MEXT, G-COE Program, and the Research Foundation for Opto-Science and Technology.

#167018 - $15.00 USD Received 18 Apr 2012; revised 25 May 2012; accepted 29 May 2012; published 22 Jun 2012